Solar Energy 266 (2023) 112144

Contents lists available at ScienceDirect

Solar Energy

journal homepage: www.elsevier.com/locate/solener

Sourcing albedo data for bifacial PV systems in complex landscapes

James C. Blakesley [a,*], George Koutsourakis [a], Daniel E. Parsons [a], Natalie A. Mica [b], Suhas Balasubramanyam [b], Mark G. Russell [b]

[a] National Physical Laboratory, Hampton Rd, Teddington, UK
[b] RINA Tech UK Ltd, Huntingdon House, North Street, Brighton, UK

ARTICLE INFO

Keywords:
Photovoltaic systems
Albedo
Bifacial photovoltaics
Yield modelling

ABSTRACT

Bifacial photovoltaic (PV) systems harvest additional light reflected from the ground. The proportion of light reflected from the ground (albedo) is a critical parameter in estimating the expected performance of these systems. It is important that albedo data are available at the system design stage are accurate and relevant, and that the confidence in these data can be quantified. This work investigates the challenges of different albedo data sources and proposes solutions towards more reliable datasets. Satellite sources, such as the NASA Moderate Resolution Imaging Spectrometer (MODIS) products, provide data that can be used to model effective albedo anywhere in the world. Nevertheless, there are numerous sources of error that can add uncertainty in bifacial gain, reducing confidence and increasing financial risk. For smaller sites (<~10 MW) located in varied landscapes, the scaling error caused by the low spatial resolution can be large. By analysing case studies in complex agricultural landscapes, we investigate the accuracy of different albedo measurement approaches. Monitoring stations with reference cells and pyranometers were deployed to validate satellite data and to realise a site measurement campaign for albedo measurements. Since these sites are much smaller than a MODIS pixel, we have evaluated alternative approaches, including “typical landscapes” with adjustments for local latitude and weather, and a novel method of combining MODIS data with higher resolution satellite data. The latter offers a practical solution with good agreement with the ground-based station.

1. Introduction

Bifacial photovoltaic (PV) technology enables light harvesting on the rear side as well as the front side of PV modules. By collecting additional light that would otherwise be lost, they increase energy production of PV systems by 5 % – 15 % [1] compared to monofacial PV. Despite being new, their market share is expected to grow from 30 % in 2022 to 50 % in 2030 [2].

Although the benefits are clear, there are still challenges for accurate prediction of the energy yield of bifacial PV systems due to the high uncertainty in modelling bifacial gain. Bifacial gain is largely dependent on the amount of light reflected from the ground. As such, models are dependent on accurate estimation of albedo for the target location. Albedo is defined as the ratio of the upwelling irradiance reflected from a surface divided by the downwelling irradiance incident on that surface. It is a property of the surface combined with lighting conditions. The large uncertainty arises from the variety of natural surfaces as well as their complexity, which includes spectral, angular, diurnal, seasonal and spatial variations. For example, previous work looking into the spectral reflectance of common surfaces and their expected effects on PV devices [3–6] predict that spectral effects alone can cause more than 25 % variation in effective rear side irradiance. Even considering only snow-free natural surfaces, albedo values can range from less than 0.1 to more than 0.5 depending on location and season. Meanwhile, natural surfaces are not isotropic (Lambertian) reflectors and often reflect relatively more light at the beginning and end of the day when sunlight is incident at a low elevation. This leads to a diurnal variation. Common PV system simulations, however, treat the ground as an isotropic reflector. Thus, a first step towards reducing bifacial gain uncertainties is by determining a reliable source of site-specific spectrally corrected albedo timeseries data with well-defined uncertainties. This is particularly important at the design phase of a PV system, when site data might not be available but where confidence in expected yield directly affects investment value.

The spectral mismatch between silicon PV devices and broadband sensors such as pyranometers is typically less than 1 % when facing the

* Corresponding author.
E-mail address: James.blakesley@npl.co.uk (J.C. Blakesley).

https://doi.org/10.1016/j.solener.2023.112144
Received 3 May 2023; Received in revised form 17 October 2023; Accepted 24 October 2023
Available online 4 November 2023
0038-092X/

sky [7], but may account for up to 25 % error for ground-reflected light [4,5]. This is because the spectrum of the light reflected from the ground is very different to the solar spectrum under which PV devices and sensors are calibrated. The mismatch is greatest for heavily vegetated surfaces, such as grass. For this reason, it is necessary to move away from a broadband definition of albedo and adopt a definition that considers the rear side spectral response of a PV device. Recently we introduced the use of "effective" albedo (a.k.a. "spectrally corrected albedo") for bifacial PV applications, where multispectral reflectance data were weighted by the rear side spectral response of bifacial PV modules, demonstrating that diurnal and seasonal spectral effects of albedo affect bifacial gain of PV systems [5]. It has also been shown that subsampling spectral albedo with only 4 wavelength channels can provide calculation of spectral mismatch with accuracy approaching that of full spectrometer measurements [4]. We define the effective albedo $\alpha^{'}$ as:

$$\alpha^{'} = \frac{\int E_{ground}(\lambda) S_{PV}(\lambda) d\lambda}{\int E_{sky}(\lambda) S_{PV}(\lambda) d\lambda} = \frac{\int \alpha(\lambda) E_{sky}(\lambda) S_{PV}(\lambda) d\lambda}{\int E_{sky}(\lambda) S_{PV}(\lambda) d\lambda} \quad (1)$$

where $E_{ground}(\lambda)$ is the global horizontal spectral irradiance reflected at wavelength λ by the ground, E_{sky} is the global horizontal spectral irradiance of the sky, S_{PV} is the relative spectral responsivity of the rear side of the relevant PV module and $\alpha(\lambda)$ is the spectral albedo of the ground. The effective albedo changes with time as lighting conditions change (solar geometry combined with atmospheric state properties, such as cloudiness, affecting radiative transfer). It can be expressed as a time-averaged quantity: hourly, daily or monthly, to simplify system modelling. In such cases, the irradiance-weighted mean (total upwelling irradiation divided by total downwelling irradiation within a period) effective albedo is used for the given time period.

A variety of satellite databases can be used to remotely observe the albedo of a site [5], with a wide range of spatial and temporal resolution data available. Gueymard *et al.* provide a comprehensive review of available satellite sources [8]. One such source is the Moderate Resolution Imaging Spectroradiometer (MODIS) database, measured with instruments onboard NASA Terra and Aqua satellites. These data have worldwide coverage and are derived from multiangle measurements of surface reflectance with filtering and averaging over 16-day periods when skies are clear. The use of such satellite databases for albedo in the context of bifacial PV systems has already been reported and evaluated in specific case studies for specific locations. For desert locations, MODIS can provide albedo estimates which are within 5 % of actual ground measurements [9]. An estimation of the errors when deriving monthly values from MODIS for use in PV system modelling for specific locations has been reported [10]. A comparison between albedo values from MODIS and ground based measurements from the Surface Radiation Budget (SURFRAD) [11] network have shown that MODIS measurements should be treated with caution as they may present differences from ground based data, particularly in more complex locations [12].

In previous published work [5], we examined the use of MODIS reflectance data [1314] to model historical effective albedo for different sites from remote observations. We used spectral interpolation of MODIS spectral bands combined with a bidirectional reflectance distribution function (BRDF) model to generate historical effective albedo values at half-hour intervals for different locations. We have validated the model at two sites using accurate *in-situ* hyperspectral surface measurements from RadCalNet [15], calculating normalised root mean squared errors (NRMSE) of about 5 % and 10 % for two sites. This work demonstrated the suitability of using the MODIS spectral BRDF product to generate historical effective albedo values for a site, specifically:

- The 7 spectral bands of MODIS provide sufficient spectral information to enable the calculation of spectrally corrected albedo values. Errors due to interpolation between bands generate relative uncertainty of the order of 1 %.
- The temporal resolution and angular information enable sufficiently accurate modelling of diurnal and seasonal variations in albedo.
- The $>$ 20 year timespan of the data can be used to quantify inter-annual variations and long term trends necessary for quantifying confidence in effective albedo forecasts.
- The 500 m pixel size and spatial resolution are sufficient for large sites in uniform landscapes, such as deserts, but cannot be used for smaller sites in complex landscapes.

Thus, MODIS is suited to providing effective albedo forecasts based on historical data as an input for yield modelling in many cases. However, there are two serious limitations to its potential accuracy:

1. Scaling effects: Scaling effects exist where the measured area is larger or smaller than the area of interest. The spatial resolution of MODIS data limits the accuracy of estimates of site albedo for smaller sites in complex landscapes. For example, across most of temperate Europe it is unusual to find fields as large as the size of a MODIS pixel. For most installations less than $\sim$ 20 MW, the site will be too small compared to MODIS pixel resolution and MODIS data will also capture neighbouring fields that will not be covered by the site. This is made worse by the point spread function of the imager [16], which spans several pixels.
2. *Anthropic* effect: Suitable land, particularly in temperate climates, is usually managed by humans to some extent. This management changes upon installation of a PV system (*e.g.* from arable to grazing), and the presence of the PV system itself may affect the *flora* or soil that determine the albedo [17,18]. The historical albedo of a site measured prior to installation of a PV system might not be a reliable guide to its future albedo following installation of that PV system. We do not address this effect further in this paper.

As a result, MODIS-derived effective albedo values are unsuitable for yield modelling or monitoring of bifacial PV systems for many locations, particularly in temperate regions. In this work, we present the challenges when using satellite data sources for albedo, specifically for applications in modelling bifacial PV systems in areas with densely packed populations or heavily used land areas. We use small (few hectare) sites as case studies to investigate the accuracy of different sources of albedo data. To provide ground-truth and compare equipment for improved albedo measurements, monitoring stations with multiple sensors were deployed at the test sites. We investigate the potential of different alternative sources of albedo data to solve this problem, including a novel combination of two satellite sources. We quantify the uncertainty of MODIS satellite data and ground-based measurements, provide statistical comparisons between sources and report on the practical limitations of each approach and proposed solutions towards useful albedo data. In Section 2 we describe the methods and the sites used in our case study. In Section 3 we describe the data analysis and sources of uncertainty for each method. In Section 4 we provide a statistical comparison between methods and describe the advantages and limitations of each approach.

2. Location and methods

2.1. Site location

Three similar grassy sites in the British and Irish Isles (50° N $\leq$ latitude $\leq 59^\circ$ N, 10° W $\leq$ longitude $\leq 2^\circ$ E) were chosen as locations for this case study (exact locations not disclosed for commercial reasons). Ground monitoring stations (described below) were installed at the sites and collected data for a period of almost 2 years from October 2020. For simplicity, we present the results of one site in the main text of this paper and the other two sites in the Supplemental Information. A satellite image of Site 1 and surrounding area is shown in Fig. 1. During the monitoring period, the field containing the site was maintained with

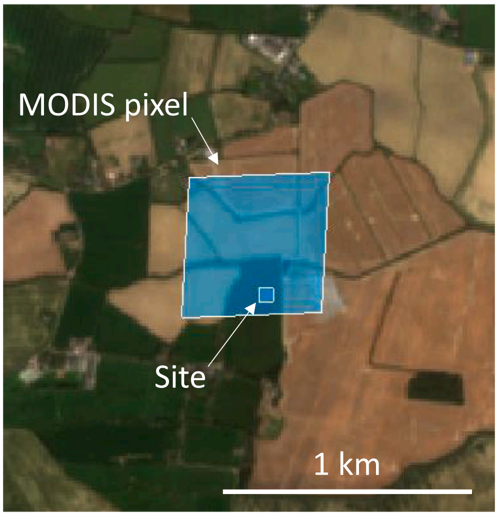

Fig. 1. Coloured image of the area surrounding the site generated from multispectral image data acquired by ESA Sentinel-2 MSI [19]. The site is located in the green field in the centre of the image, highlighted by the small blue square. The approximate boundary of the nearest MODIS pixel is shown by the large blue parallelogram.

regular mowing of the grass, but no tilling or sowing. This was to simulate conditions similar to those used for a PV system. The site field is smaller than the size of a 500 m × 500 m MODIS pixel. Hence, the signal from the MODIS pixel containing the site is dominated by the surrounding land, which is a mixture of crops and grazing farmland.

The site has a mild temperate maritime climate, dominated by westerly winds bringing Atlantic weather systems. As a result, the site is mostly cloudy or overcast more than 50 % of the time. The sky is completely clear only about 15 % of the time. These features combined present an almost worst-case scenario for estimating effective albedo using remote sensing: The complex landscape presents issues for imaging with moderate resolution satellites, such as MODIS, while the high cloud cover limits the number of days on which good observations are possible. Due to the abundant vegetation, we also expect significant spectral and seasonal effects. Thus, the site provides an ideal case study for the use of alternative or combined albedo data sources for challenging locations.

2.2. Ground-based measurements

Ground-based measurements can provide the most specific and accurate measurement of albedo. However, they require land to be set aside and managed for long enough to capture relevant seasonal trends, which would ideally be for at least one year. This is generally impractical for pre-installation yield assessments of PV projects, though ground-based albedo measurements are used for monitoring performance ratios of bifacial PV systems [20] where they are installed alongside PV systems. In this study the ground-based measurements provide a ground truth against which we can compare alternative sources of albedo data.

We installed one ground-monitoring station at each site using instrumentation that met or exceeded the requirements for a class A monitoring system defined by IEC 61724-1 [20]. The systems included a pyranometer albedometer and a reference cell albedometer. Each albedometer comprised a pair of sensors mounted horizontally back-to-back, with one of each pair facing the sky and the other facing the ground. The sensors were Hukseflux SR20-D2 secondary standard pyranometers and IMT Solar Si-RS485TC-T temperature-compensated reference cells. The sensors were mounted at a height of about 1.8 m above ground level on a horizontal pole cantilevered from a mast. They were connected to a datalogger equipped with communications module, battery and solar charger. The sensors were sampled at 5 s intervals, with the mean and standard deviations of 12 samples recorded at 1 min intervals.

The approximate spectral response and angular response of the two types of sensors are shown in Fig. 2. The pyranometer responds to the entire short-wave radiation spectrum from 280 nm to 3000 nm. Being a thermal radiation sensor, it has a flat response in terms of output per unit irradiance. On the other hand, the reference cell has a spectral response that is similar to that of a PV module, potentially enabling the measurement of effective albedo instead of broadband albedo. One problem of the reference cell, however, is that reflections from its planar glass cover significantly reduce the measured effective irradiance at high angles of incidence. This effect can be modelled approximately using incident angle modifier (IAM) models. In Fig. 2 we show the result of fitting the 1-parameter Martin and Ruiz IAM model [23] to the reference cell angular response using a parameter $a_r = 0.163$. This enables an angular correction to be applied, albeit with the introduction of significant uncertainty. We discuss the implications of the angular and spectral effects further in section 3.1.

2.3. MODIS BRDF parameters

The NASA MODIS product MCD43 [14] provides BRDF parameters for 7 narrow spectral bands from 455 nm to 2155 nm. These parameters describe the angular dependence of reflectance. They are a level-3 data product derived by fitting a 3-parameter BRDF model to a set of remote sensing observations taken from multiple angles and times over a 16 day period. The parameters are reported at daily intervals at a surface spatial resolution of 500 m. The MODIS BRDF parameters enable the estimation of historical effective albedo anywhere on the globe for any date from the year 2000.

In principle, the calculation of albedo from BRDF requires the 5-dimensional integration of the product of spectrally and angularly resolved incident radiance with the spectrally resolved BRDF. This is complex and requires more information than is typically available. For simplicity, it is convenient to separate into two components: White-sky albedo α_{ws} and black-sky albedo α_{bs}, representing diffuse and direct illumination components respectively. α_{ws} is calculated from a bi-hemispherical integral of the surface BRDF assuming an isotropic light source (diffuse sky). α_{bs} is calculated from a single hemispherical integral of the BRDF assuming that all incoming light is from a single direction (the Sun). α_{bs} is a function of solar zenith angle θ_{Sun}, whereas α_{ws} is independent of the Sun's position. The total albedo α estimated from a weighted sum of these sources:

$$\alpha = k_{diff}\alpha_{ws} + (1 - k_{diff})\alpha_{bs} \quad (2)$$

where k_{diff} is the quotient of diffuse horizontal irradiance (DHI) divided by global horizontal irradiance (GHI). We used this approach to estimate effective albedo using the following procedure:

1. Download 20 years of daily BRDF parameters for the MODIS pixel containing the site.
2. For each day of the 20 year period calculate the narrow band white sky albedo α_{ws} for each MODIS spectral band. We used the polynomial expression described in reference [24] instead of full numerical integration of the BRDF.
3. For each minute in each day, calculate θ_{Sun}. We used NREL's Solar Position Algorithm [25]. Occasions where $\theta_{Sun} > 80^{\circ}$ are omitted. (BRDF reconstruction is inaccurate for $\theta > 80^{\circ}$.)
4. For each minute, use the MODIS BRDF parameters with incident angle θ_{Sun} to calculate the narrow band black sky albedo α_{ws} for each spectral band. We used the polynomial in [24].
5. Estimate the expected GHI, DHI and k_{diff} for each minute (see below).
6. Use Eq. (2) to calculate the total narrow band albedo for each spectral band for each minute.

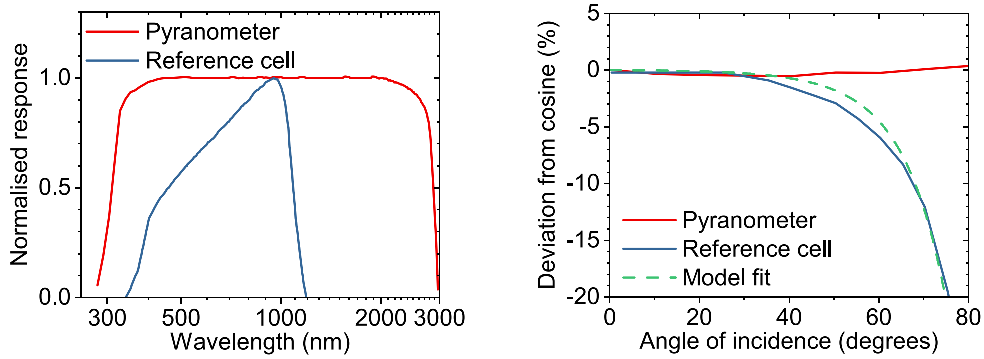

Fig. 2. Comparison of sensor performance characteristics using data extracted from manufacturers' datasheets [21,22]. Left: Normalised spectral responsivity (x axis on logarithmic scale). Right: Angular response deviation from ideal cosine behaviour. The blue dashed line shows a model fit to the reference cell angular response using the Martin and Ruiz incident angle modifier model [23].

7. For each minute, convert the 7 narrow band albedo values into spectrally corrected broadband (effective) albedo values α' using Eq. (1). To perform the integration, a spectral albedo function is created by interpolation of the MODIS spectral bands.
8. Hourly, daily and monthly time-averaged effective albedo values are created by calculating the GHI-weighted mean albedo value within each period.

This method has been validated previously for highly uniform landscapes [5]. To perform this calculation, one requires daily BRDF parameters, GHI and DHI data at 1 min resolution, spectral irradiance of the sky hemisphere $E_{sky}(\lambda)$ and spectral responsivity of the relevant PV device $S_{PV}(\lambda)$. In this study we use the AM1.5G reference spectrum [26] for $E_{sky}(\lambda)$, . Deviations of the sky spectrum from the reference have a small impact on effective albedo, which is included in our uncertainty budget. Nevertheless, it is convenient to use this reference spectrum as it is also used for calibration of PV reference devices. For $S_{PV}(\lambda)$ we use the spectral response of the reference cell shown in Fig. 2. This emulates a hypothetical scenario in which a reference cell has been chosen to match the rear side spectral response of the proposed bifacial PV array.

For this study we chose to emulate the common case in which local ground-based measurements of GHI and DHI are not available. For many regions of the globe historical modelled irradiance data are available at various time and spatial resolutions from sources such as the National Solar Radiation Database (NSRDB) [27] and European Centre for Medium Range Weather Forecasting (ECMWF) [28]. For long-term forecasting, typical meteorological year (TMY) data from commercial sources are often used. In this study, however, we use a simple constant cloud-cover model to generate irradiance data. Firstly we use the Bird clear sky model [29] to generate clear sky GHI values $G_{clearSky}$ for each minute in the year. Secondly, we multiply this by a cloud cover index k_{cloud} to generate the cloudy sky GHI: $G_{cloudySky} = k_{cloud}G_{clearSky}$. Finally we use the correlation model of Reindl, Beckman and Duffie to estimate the DHI and k_{diff} from $G_{cloudySky}$ [3031]. The uncertainty in albedo arising from estimation of irradiance and k_{diff} is included in our uncertainty budget. We used a value of $k_{cloud} = 0.83$ obtained by calculating the irradiance-weighted mean clear-sky index from recorded GHI data.

The MODIS-derived effective albedo values were used in two different ways: Historical data and forecast data. The historical data are the last 20 years of data generated as described above, representing an estimate of the actual effective albedo recorded at the site for times in the past. The forecast albedo is an estimate of the likely albedo at the site for times in the future. We generated a "forecast albedo year" at hourly, daily and monthly resolutions using the mean albedo values from the same hour-of-year, day-of-year or month-of-year of each of the previous 20 years. The standard deviation of these 20 values for each period is included in the forecast uncertainty budget as the interannual variation.

2.4. "Typical landscape" datasets

When the spatial resolution of MODIS is insufficient to accurately image the target site, a potential alternative studied in this work is to use a different "typical landscape" as a reference. The typical landscape should have the same ground type and seasonal behaviour as the target site. In that case, reflectance data from the typical landscape could be used in place of data from the actual target site. For this study we generated a "typical" temperate grassy BRDF parameter dataset sourcing data from MODIS satellite observations of 5 different sites. The sites (2 in Europe, one in North America, one in South America and 1 in New Zealand) were chosen to meet the following criteria:

- Temperate latitude (approximately ± 40° to ± 50°).
- Covered with grass or other low, green vegetation and uniform over a much larger area than a single MODIS pixel.
- Negligible area covered by trees, buildings, roads or other non-vegetated surfaces.
- Grazed naturally or by farm animals.
- No change in land use over the past 10 years.

We extracted the MODIS BRDF parameters for the past 10 years from each site. These parameters were all combined from all these sites and used in place of the site MODIS BRDF parameters to generate a "typical landscape albedo year" using the method described in 2.3. Note that we used the location and weather data from the target site rather than the "typical landscape" locations. This is equivalent to translocating the surface from the typical landscapes to the target site. The translocation is necessary because albedo is a property of both the surface and the illumination conditions; an identical surface has different albedo values in different locations. The mean effective albedo of all "typical landscapes" was used to generate the "typical landscape albedo year" for the site, and the standard deviation between the landscapes was used to estimate the uncertainty from variations in different types of grassy surface and different seasonal patterns.

2.5. Hybrid satellite data

The European Space Agency (ESA) Copernicus Sentinel-2 Mission [32] comprises two satellites in sun-synchronous polar orbits. Their main instrument is the Multispectral Instrument (MSI). This records images of the Earth's surface in 13 narrow spectral bands spanning 440 nm to 2200 nm. The MSI images a narrower swath than MODIS. As a result, it achieves higher spatial resolution images with 20 m × 20 m pixel sizes available. However, there are two main limitations compared to MODIS. Firstly, sites are visited less frequently, typically once every 5 days. Secondly, sites are only imaged from a narrow range of zenith angles close to nadir and at times close to solar noon. There is no level–3 daily BRDF parameters data product from the MSI as this would require multiple observations from a broader range of observations and solar zenith angles. Instead, a lower-level data product (level-2 MSIL2A) provides snapshot reflectance images at infrequent intervals. It is not possible to use these data alone to generate albedo values as the angular dependence of reflectance is unknown.

We present and test a new method to combine the high spatial resolution of Sentinel–2 with the better time resolution and angular reflectance information available at lower spatial resolution from MODIS. The method is based on an assumption that the shape of the BRDF is approximately homogeneous and varies only in magnitude within a MODIS pixel. To generate the hybrid satellite albedo data, we first generate the historical MODIS effective albedo for the site as described in the previous sections and we then modify these values according to Sentinel-2 observations. We assume that the angular dependency of reflectance for the MODIS pixel is representative of that of the site. Therefore, the ratio of albedo between the site and the MODIS pixel is assumed to be the same as the ratio between the reflectance of the site and the reflectance of the MODIS pixel. Explicitly:

$$\frac{\alpha'_{site}(t)}{\alpha'_{MODIS}(t)} \approx \frac{r'_{site}(\theta_{Sun}, \theta_{obs}, \phi, t)}{r'_{MODIS}(\theta_{Sun}, \theta_{obs}, \phi, t)} \tag{3}$$

where $\alpha'_{site}(t)$ and $\alpha'_{MODIS}(t)$ are the spectrally corrected albedos for the site area and the MODIS pixel respectively at time t, and $r'_{site}(\theta_{Sun}, \theta_{obs}, \phi, t)$ and $r'_{MODIS}(\theta_{Sun}, \theta_{obs}, \phi, t)$ are the values of reflectance observed for the site and MODIS pixel respectively at time t with θ_{obs} being the zenith angle of the observer and ϕ being the azimuth angle between Sun and observer. This assumption can be used to provide estimates of site albedo at the times of good Sentinel 2 observations. However, interpolation is required to fill gaps between these times. $\alpha'_{site}(t)$ cannot be directly interpolated as it is influenced by diurnal and weather variations and is not a smooth function. Instead, we assume that effective white-sky albedo $\alpha'_{ws,site}$ of the site varies slowly with time such that it can be approximated by a linear interpolation in time between good observations from the Sentinel-2 satellite. For time t in the interval $t_i \leq t \leq t_{i+1}$:

$$\alpha'_{ws,site}(t) = \frac{(t_{i+1} - t)\alpha'_{ws,site,i} + (t - t_i)\alpha'_{ws,site,i+1}}{t_{i+1} - t_i} \tag{4}$$

where t_i is the time of the i^{th} good Sentinel-2 observation and $\alpha'_{ws,site,i}$ is the corresponding white-sky albedo observation for the site:

$$\begin{aligned}\alpha'_{ws,site,i} &= \alpha'_{ws,MODIS}(t_i)\frac{r'_{site}(\theta_{Sun,i}, \theta_{obs,i}, \phi_i, t_i)}{r'_{MODIS}(\theta_{Sun,i}, \theta_{obs,i}, \phi_i, t_i)} \\ &\approx \alpha'_{ws,MODIS}(t_i)\frac{r'_{S2,i}}{r'_{MODIS}(\theta_{Sun,i}, 0, 0, t_i)}\end{aligned} \tag{5}$$

where $r'_{S2,i}$ is the spectrally corrected broadband reflectance of the site observed by Sentinel-2 at time $t_i \leq t \leq t_{i+1}$ and we use the BRDF functions described in [24] with the MODIS BRDF parameters to calculate the nadir reflectance $r'_{MODIS}(\theta_{Sun,i}, 0, 0, t_i)$ and white-sky albedo $\alpha'_{ws,MODIS}(t_i)$ for the MODIS pixel at time t_i. The procedure for generating hybrid satellite albedo data for the site is:

1. Generate MODIS historical effective albedo values $\alpha'_{MODIS}(t)$ and white-sky albedos $\alpha'_{ws,MODIS}(t)$ for the MODIS pixel containing the site.
2. Identify good Sentinel-2 observations of the site that include the specific area of interest.
3. Extract reflectance values from each spectral band of Sentinel MSIL2A for the site area for each cloud- and shadow- free observation.
4. Apply spectral interpolation and weighted integration, as Eq. (1), to convert the narrow band Sentinel-2 reflectance values to spectrally corrected reflectance observations $r'_{S2,i}$.
5. Calculate the corresponding $r'_{MODIS}(\theta_{Sun,i}, 0, 0, t_i)$ from MODIS daily BRDF parameters.
6. Construct a linear interpolant $\alpha'_{ws,site}(t)$ from the points $(t_i, \alpha'_{ws,site,i})$ using (4) and (5).
7. Modify the MODIS data by the interpolant to generate $\alpha'_{s2:MODIS,t} = \frac{\alpha'_{MODIS}(t_t)}{\alpha'_{ws,MODIS}(t_t)}\alpha'_{ws,site}(t_t)$ for the hourly, daily or monthly interval t_t.

We downloaded MSIL2A image tiles [19] containing the specific site of this work, for the period from January 2020 to October 2022. Tiles with cloud cover greater than 50 % were not downloaded. In total 78 images were downloaded, averaging about 1 image per 13 days, although the distribution was skewed towards summer months due to seasonal cloud cover variation. Of these images, a smaller subset of pixels covering the ground monitoring station were extracted, and the mean reflectance in each spectral band was calculated from these. A second level of filtering (described in section 3.3) was necessary to further reject poor observations due to obfuscation of the Sun or satellite by clouds, eliminating about 80 % of the downloaded images in total. This demonstrates the limitations of using Sentinel-2 data alone for use in PV applications where high temporal resolution is required. The same inputs for irradiance, spectral irradiance and spectral responsivity were used as in section 2.3.

The Sentinel-2 MSIL2A data are only available from 2018 onwards. A longer period would be preferred to generate sufficient statistical information required for meaningful forecasting. Hence we did not produce an albedo forecast using combined Sentinel-2 and MODIS data, but produced only historical albedo estimates for the period of the study.

3. Results and uncertainty analysis

3.1. Ground-based measurements

Irradiance measurements from the ground-based sensors were used to generate hourly, daily and monthly irradiance-weighted albedo values α_t.

$$\alpha_t = \frac{\sum_{i\in t} G_{ground,i}}{\sum_{i\in t} G_{sky,i}} \tag{6}$$

where $G_{sky,i}$ and $G_{ground,i}$ are the horizontal irradiance measured at minute i on the sky and ground facing sensors respectively and $t = (hourn, dayn, ormonthn)$ is the relevant period. For each datapoint, we estimated the solar zenith angle using the Bird model [29]. Data points where $\theta_{Sun} > 90^\circ$ (night-time) were excluded from binning. We developed a simple measurement uncertainty model based on that proposed by Hukseflux and NREL [33] and using manufacturers' instrument specifications. The model includes uncertainties due to correlated relative errors (calibration, stability, linearity, temperature, tilt, drift), absolute errors (logger accuracy, offset) and angular dependent errors (directional response) and statistical (type A) sources related to noise, sky variability and thermal transients. The uncertainty was calculated for each record and combined, using standard methods [34], including the effect of correlations. The resulting measurement uncertainty is dynamic and depends on contemporary measurement conditions (period duration, irradiance, direct/ diffuse light ratio, Sun angle). In general, the measurement uncertainty from the reference cells was similar to that of the pyranometers. An example breakdown of uncertainty sources is shown in Table 1.

Fig. 3 shows the monthly averaged albedo for the entire measurement campaign and an example of hourly averaged albedo measured over one day. Correlations and differences between different sensor

Table 1
Breakdown of relative combined uncertainty (1 standard deviation) for each sensor type for the sum of irradiance values measured over the month of April 2021. * The angular-dependent uncertainty shown here is for the case of angular-response corrected measurements.

Uncertainty component	Pyranometer (sky)	Pyranometer (ground)	Reference cell (sky)	Reference cell (ground)
Absolute correlated	0.61 %	2.30 %	0.82 %	2.78 %
Relative correlated	0.92 %	0.92 %	1.25 %	1.25 %
Angle correlated	1.11 %	1.16 %	0.69 % *	0.06 % *
Type A uncorrelated	0.02 %	0.02 %	0.02 %	0.02 %
Total $\boldsymbol{u}(\boldsymbol{G}_t)$	1.56 %	2.74 %	1.65 %	3.05 %

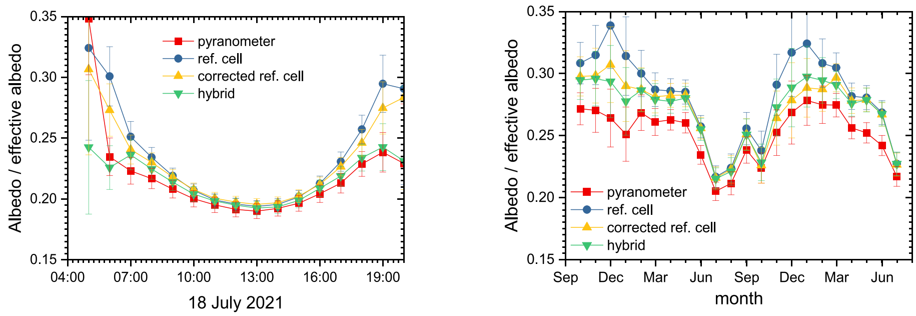

Fig. 3. Ground-based albedo measurements using different combinations of ground-based sensors. Left: Hourly-averaged values measured on one clear summer day. Right: Monthly-averaged values measured over a 2-year period. Error bars show 1 standard deviation measurement uncertainty.

types appear as expected. The hourly data show a typical diurnal variation, in which the albedo is lowest when the elevation of the Sun is at its highest. The monthly data shows a repeated seasonal variation, where the albedo is lowest in the summer and higher in the winter. The measurement uncertainty is also considerably higher in the winter due to high cloud cover, short days and high solar zenith angles.

Comparing albedo measurements from different sensor types reveals systematic differences. Values obtained from the pyranometer albedometer are consistently lower than those obtained by the reference cell albedometer. This is caused by the spectral and angular response differences shown in Fig. 2. Firstly, the dense vegetation influences the spectrum of the reflected light, causing a spectral mismatch between the ground-facing sensors. This increased the albedo measured by the reference cell albedometer by about 5 % to 10 % relative to the pyranometer albedometer. This difference is consistent with the expected spectral correction for grass surfaces [5,35]. Secondly, reflections from the planar glass surface of the reference cell results in an underestimate of the direct downwelling irradiance under high θ_{Sun}. This causes a corresponding increase in the apparent albedo measured by the reference cell albedometer. As this effect depends on the angle of the Sun, it is more prominent in winter and around dawn and dusk.

To obtain a ground-based measurement of spectrally corrected effective albedo relevant to bifacial PV systems, we need to combine the spectral response of a matched reference cell with the flat angular response provided by the pyranometer sensors. We propose two ways to achieve this. In the first, we modify the reference cell albedometer measurement with an angular-response correction to reference cell irradiance measurements:

$$G'_{sky} = \frac{G_{sky}}{k_{diff} f_{IAM,diff} + (1 - k_{diff}) f_{IAM}(\theta_{Sun})}$$
$$G'_{ground} = \frac{G_{ground}}{f_{IAM,diff}} \tag{7}$$

where G'_{sky} and G'_{ground} are the incident-angle corrected irradiances measured, derived from the sky-facing and ground-facing reference cell measured irradiances G_{sky} and G_{ground}, respectively. k_{diff} is the diffuse light fraction, $f_{IAM}(\theta)$ is the incident angle modifier (IAM) function for direct light, and $f_{IAM,diff}$ is the IAM for diffuse light. We used the Martin and Ruiz [23] IAM model with fit parameter $a_r = 0.163$ and $f_{IAM,diff} =$ 0.986 derived by assuming isotropic diffuse radiance. As θ_{Sun} and k_{diff} are not measured directly, they were inferred from calculation [29] and estimation [30] respectively, using location, time and GHI as inputs. This method is relatively complex to implement and relies on estimation and assumptions.

The second method is referred in this work as the “hybrid albedometer” method. In this method we combine the measurements of the sky-facing pyranometer with the ground-facing reference cell:

$$\alpha'_{hybrid} = \frac{G'_{ground,refCell}}{G_{sky,pyranometer}} \tag{8}$$

where $G'_{ground,refCell}$ is the angle-corrected ground-facing reference cell irradiance measurement and $G_{sky,pyranometer}$ is the uncorrected sky-facing pyranometer reading. This method uses the best aspects of both sensor types, summarised in Fig. 4. The reference cell applies spectral correction to coloured light reflected from the ground while the diffuse nature of the reflected light minimises the angular response error. The flat angular response of the pyranometer minimises IAM errors in direct sunlight, while the spectral mismatch error between the pyranometer and PV module is small when the sky spectrum is close to the AM1.5 reference spectrum. As shown in Fig. 3, both methods agree with each other to within estimated uncertainty, demonstrating the suitability of either method for measuring effective albedo and its agreement with the angular-response correction.

3.2. MODIS effective albedo data

Fig. 5 compares the effective albedo measured from the hybrid albedometer to the different predictions generated using MODIS BRDF parameters. These include the historical satellite data from the MODIS pixel containing the site, the forecast value based on the statistics of the previous 20 years, and the “typical landscape” forecast using 10 years of MODIS observations of alternative, more uniform, temperate grassy sites. Within a single day, the MODIS BRDF model reproduces the diurnal variation measured from ground-based measurements. However, there is no significant correlation with ground-based measurements for daily or monthly effective albedo values observed by MODIS for the site area. Most of the time, the error between MODIS and ground-based measurements of effective albedo was greater than the estimated

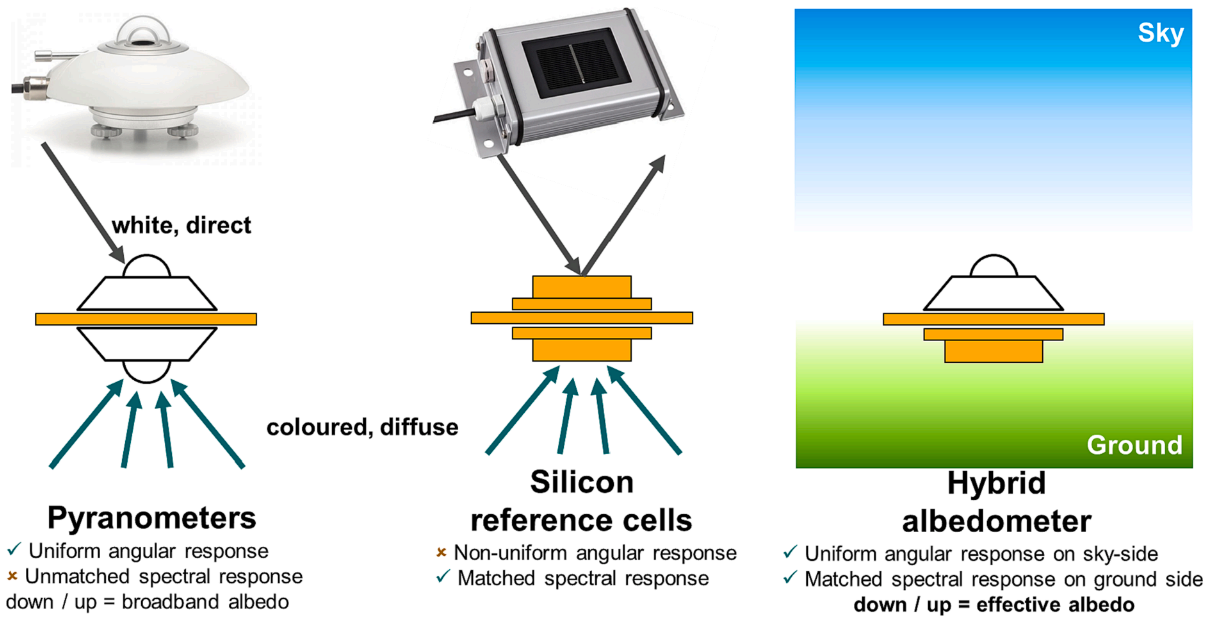

Fig. 4. Schematic summarising the advantages and disadvantages of different sensor combinations for measuring albedo.

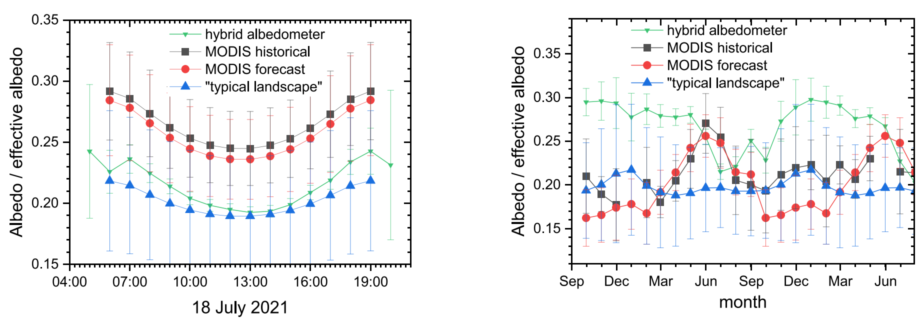

Fig. 5. Effective albedo generated from MODIS BRDF parameters for the site. Black squares and red circles are generated for the MODIS pixel containing the site using historical and statistical forecasting respectively. Blue triangles are generated using MODIS BRDF parameters from other "typical landscape" grassy locations. The ground-based measurements of the hybrid albedometer are shown for reference. Left: Hourly-averaged values measured on one clear summer day. Right: Monthly-averaged values measured over a 2-year period. Error bars show 1 standard deviation measurement uncertainty.

measurement uncertainty. This is simply because the MODIS pixel is dominated by the fields surrounding the site, which were predominantly used for crops. Indeed, a typical summer-crop farming cycle profile is visible in the MODIS site forecast data; the significant increase around June is likely caused by the higher albedo from growing, green cropland.

The "typical landscape" forecast also bore very little correlation to the ground-based measurements. This forecast was generated from the mean of 5 sets of BRDF parameters taken from different locations around the world. The effective albedos created from each individual location's parameters are shown in Fig. 6. The typical landscape datasets reveal a diverse range of effective albedo values and seasonal patterns. It is clear from these results that there is too much variety in temperate grassy landscapes to use "typical" values at this level; more detailed classification of sites is required, such as soil type, flora and microclimate information. The very large uncertainties attributed to the typical landscape forecast arises mostly form this variation between locations.

We developed a comprehensive uncertainty model for generating historical and forecast effective albedo from MODIS BRDF parameters. The basic accuracy of the MODIS albedo product was estimated from an analysis of previous validation exercises [5,16,36–38]. The MODIS data specification [39] includes quality flags indicating whether observations were sufficient to achieve a good fit to the BRDF model. Best practice is to focus on best quality data. However, in the locations used in this

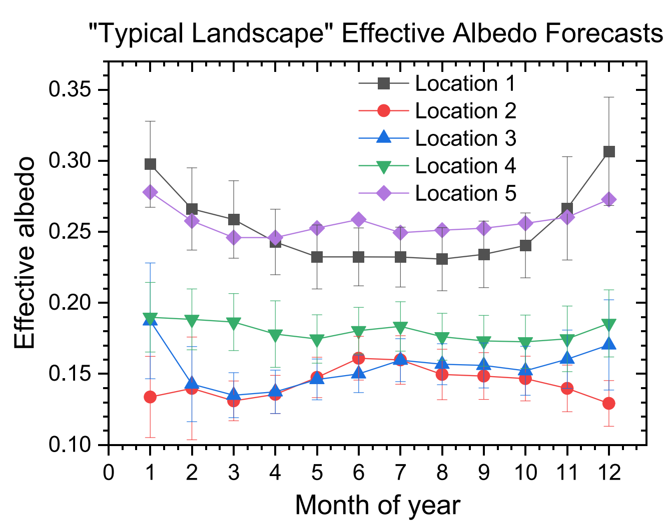

Fig. 6. Monthly effective albedo generated from MODIS BRDF parameters from 5 different "typical landscape" temperate grassy locations. Error bars indicate 1 standard deviation uncertainty including interannual variation.

work, cloudy skies sometimes limit the number of good observations. To avoid data gaps, we included imperfect quality data in our analysis with an additional uncertainty component whose magnitude was based on an analysis of the correlation between quality flags and measurement error in ground-truth studies. To this we added model-based estimates of the effects of spectral interpolation errors, uncertainty in the estimation of k_{diff}, uncertainty in PV module (reference cell) spectral responsivity, deviation of the spectral irradiance from the reference spectrum, and geometric effects from anisotropic reflectance.

For albedo forecasts, we also included an estimate of forecast uncertainty based on interannual variation over the previous 20 years, and for the typical landscape forecast we also included the inter-location variation. A summary of the different contributions for the month of April 2021 is given as an example in Table 2.

3.3. Hybrid satellite data

We generated effective albedo measurements from the combination of MODIS and Sentinel-2 satellites using the method described in 2.5. Initially Sentinel-2 images were filtered using the pixel classification scheme provided with the MSIL2A product to remove any pixels containing cloud or cloud shadows. However, the remaining dataset contained many outliers and the agreement with the ground-based measurements was not significantly improved relative to using MODIS data alone. Visual inspection of the data showed that the poor performance was caused by poor quality Sentinel–2 observations that were partly obscured by cloud, cloud shadows or haze. This was greatly improved by adding a second level of filtering. We tested two alternative methods of filtering. In the first we used the GHI timeseries data from the ground-based pyranometer to automatically identify periods of clear skies [4041]. Sentinel-2 images not coinciding with clear sky times were rejected. In the second method we visually inspected each Sentinel-2 image and rejected any images that were judged to be of poor quality. Both methods performed well, but the manual inspection approach provided the best agreement with ground-based measurements. The effective albedo values generated using the latter approach are shown alongside ground-based measurements in Fig. 7. The observed diurnal trends and some of the seasonal trends of the ground-based measurements were recreated by this method, albeit with added random variations. With some additional filtering and more historical data, this method is promising for generating accurate albedo forecasts.

4. Comparison

To quantitatively compare the different methods, we compiled statistical summaries of the irradiance-weighted RMS uncertainty and mean-bias error (MBE) and normalised root-mean squared error (RMSE) relative to the “ground truth” of the hybrid albedometer measurements. These results are shown in Table 3. The uncertainties are an average over the whole 2 year period; higher uncertainties were recorded in winter months and lower in summer months due to seasonal variations in the daily irradiation and zenith angle. To summarise, we found that the hybrid albedometer and angular response corrected reference cell albedometer methods agreed to within the estimated measurement uncertainty. The pyranometer albedometer was significantly biased to lower values due to spectral mismatch compared to silicon cells. The uncorrected reference cell measurement suffered from a positive bias error, especially in hourly data, from angular response effects. Nevertheless, all ground-based measurements were, as expected, more accurate than remote sensing approaches.

MODIS satellite measurements achieved average uncertainty on monthly values of about 10 % for the whole MODIS pixel. However, the NRMSE values (>25 %) reveal the very large scaling error between the large MODIS pixel and the smaller site. Using the combination of Sentinel-2 and MODIS satellites reduced the NRMSE to just 10.1 % in the case of monthly average albedo, and a mean bias error of only −4.5 %. This is a remarkable result, although we stress that the NRMSE values are specific to this site only. The study was repeated at two more sites (shown in the Supplemental Information), which produced similar results. However, all three sites were in similar locations.

At this stage we caution against generalising the method to any location until further validation is performed with additional sites that represent a larger variety of conditions. In particular, the hybrid satellite method assumes that the shape of the BRDF is homogeneous on the scale of a MODIS pixel. This may not be valid where there is a variety of surface geometries (*e.g.* cropland mixed with forest) within or around the MODIS pixel. Nevertheless, considering the site size and complexity, the results of this work present a promising route towards reliable remote sensing albedo data acquisition for bifacial PV systems yield forecasting.

Table 2
List of contributions to uncertainty in monthly-averaged MODIS-derived effective albedo, using April 2021 as a typical example. Values shown are relative standard deviations rounded to 2 significant figures.

Uncertainty source	MODIS site historic (%)	MODIS site forecast (%)	Typical landscape forecast (%)
MODIS BRDF base accuracy	7.5	4.2	4.2
Spectral interpolation	0.98		
k_{diff} estimation	3.30		
PV Spectral responsivity	0.50		
Spectral irradiance variation	3.00		
Geometric effects (anisotropy)	6.20		
Temporal interpolation	0.00		
Location variation	N/A	N/A	29.0
Forecast uncertainty (interannual variation)	N/A	4.0	3.6
Combined uncertainty $u(\alpha')$	10	10	30

5. Conclusions

In conclusion, we have investigated the use of different sources of albedo data for the purposes of yield modelling and monitoring for bifacial PV systems. We used particularly challenging sites as case studies, which suffer from a complex surrounding landscape, high latitude and heavy cloud cover. Ground-based measurements provided the most accurate measure of albedo of the sites, but are impractical to implement, requiring at least one year to reproduce seasonal trends. As well, during this period the sites must be maintained as a PV installation. This is impractical for many PV yield assessment applications, although it could be useful for bifacial PV system monitoring.

We showed that a pyranometer-based albedometer introduced a bias by measuring broadband shortwave albedo instead of the spectrally corrected effective albedo relevant to bifacial PV systems. A reference cell pyranometer, on the other hand, overestimated effective albedo due to reflective losses at high solar zenith angles. Our proposed solution is to use a “hybrid albedometer” combining a sky-facing pyranometer with a ground-facing reference cell whose spectral response is matched to the rear side spectral response of the relevant PV module. This method measured effective albedo with an uncertainty of about 5 % (one standard deviation). It also has the advantage of being compatible with the requirements of IEC 61724–1:2021 PV system monitoring standard [20].[20]. A slightly lower cost alternative uses back-to-back reference cells with an angular response correction applied. However, the latter method was more complex to implement and less accurate on shorter timescales due to errors in the estimation of diffuse irradiance.

The use of MODIS satellite BRDF parameters has been shown to generate effective albedo values with accuracies of better than 10 % for sites that are uniform on a scale larger than the 500 m MODIS pixel. This

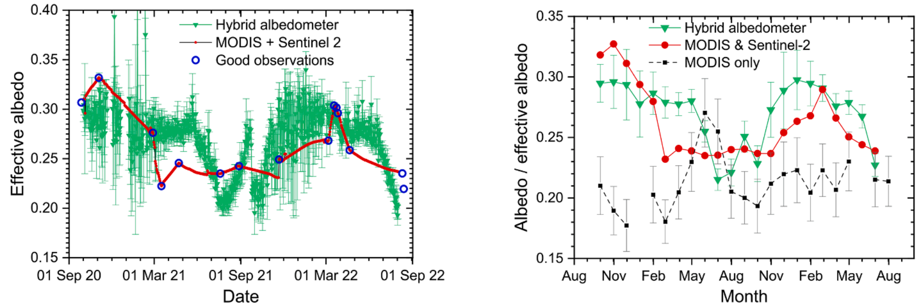

Fig. 7. Daily (left) and monthly (right) effective albedo generated by combining MODIS and Sentinel-2 satellite data from the site (red dots). The ground-based hybrid albedometer readings are shown for comparison (green triangles). The days coinciding with good Sentinel-2 observations are highlighted by blue circles. Intermediate days are generated by interpolation (Eq. (4)). The monthly albedo generated from MODIS alone (from Fig. 5) is shown for comparison.

Table 3
Statistical comparison of different sources of albedo data for the site over the period from October 2020 to July 2022. RMS uncertainties are expressed as one standard deviation. NRMSE values relative to the hybrid albedometer "ground truth". Statistics were calculated for hourly, daily and monthly averaging periods. Note that at present we do not have a method for estimating uncertainty for the hybrid satellite approach.

Method	Mean α'	MBE (%)	Hourly		Daily		Monthly	
			Uncertainty $u(\alpha')$ (%)	NRMSE (%)	Uncertainty $u(\alpha')$ (%)	NRMSE (%)	Uncertainty $u(\alpha')$ (%)	NRMSE (%)
Hybrid albedometer	0.262	–	6.1	–	5.0	–	4.7	–
Pyranometers	0.244	−6.7	5.3	8.5	4.4	8.1	4.2	7.6
Reference cells	0.269	2.4	6.3	8.4	5.0	5.4	4.8	3.5
Corrected ref. cells	0.263	0.4	6.0	5.5	4.9	3.0	4.6	1.3
MODIS site historic	0.224	−15.2	15.5	27.8	12.5	25.7	10.7	25.4
MODIS site forecast	0.224	−14.9	15.5	28.0	14.2	28.3	12.0	27.6
"Typical landscape"	0.194	−25.7	29.6	38.1	29.0	37.8	28.1	37.3
Sentinel-2 & MODIS	0.250	−4.5	unknown	12.3	unknown	11.5	unknown	10.1

method has the advantages of using free data with more than 20 years of global coverage and is suitable for many locations. However, for complex landscapes, such as those sites studied here, large scaling errors are introduced. In this case seasonal trends were not reproduced at all by MODIS, and relative errors in effective albedo were typically greater than 25 %. We also explored the use of using other grassy temperate sites to provide "typical landscape" datasets. However, we found that there was too much variety in albedo between one grassy site and another for such a simple generalisation to prove accurate. The "typical landscape" approach produced the worst results with errors approaching 40 %.

We introduced a new approach of combining the higher spatial-resolution reflectance measurements of Sentinel-2 satellites with the higher frequency MODIS observations to generate a hybrid satellite measurement of effective albedo. In this particular case study, the method proved remarkably good at agreeing with ground-based measurements. It achieved NRMSE of nearly 10 % despite the very cloudy location. This method was more complex to implement than the using MODIS satellites alone, and requires improvements to automatic filtering methods to avoid the need for manual sifting of satellite observations. Sentinel-2 also provides less than 5 years of historical data at present. In principle, NASA Landsat satellites could also be used to increase coverage and extend over a longer historical period. Nevertheless, the method shows great promise for remote estimation of effective albedo for bifacial PV systems in complex landscapes and its suitability for providing highly localised effective albedo forecasts deserves further exploration. However, we reiterate that we have only validated it for specific dense cropland landscapes and note that the assumptions might fail in the case of heterogeneous landscapes such as mixed forest/cropland or in the presence of snow.

Note that an assumption of this paper is that albedo is the relevant quantity for PV system modelling. This is on the basis that PV system models usually assume that the ground is an isotropic (Lambertian) scattering surface. However, our results indicate significant deviations from isotropic behaviour. When applying albedo measurements of estimates to PV systems yield modelling, it may be necessary to also consider angular and geometric effects. As PV arrays are tilted, have an angle-dependent response and create shadows, they are more sensitive to some angles of reflections than others. By contrast, albedo is a measure of hemispherical irradiance ratio in a horizontal plane. Typically, PV systems models assume an isotropic scattering ground surface, whereas most natural surfaces are non-isotropic reflectors that can be described by a BRDF. An ideal simulation would include extending beyond scalar albedo values to include full BRDF modelling and more sophisticated sky models. The difference in bifacial gain between full BRDF and isotropic reflectance models depends on the system design (tracker or fixed, tilt angle, relative ground clearance). We estimate the typical relative error due to these geometric effects to be of the order of 5 % to 10 %, but a full investigation is beyond the scope of this paper.

Finally, we reiterate that, for any PV installation, the PV system itself, the act of installation and the associated change of land use all have impacts on the ground and vegetation. This will affect albedo values in an unpredictable way, in the short-term period after installation but also the long term, since it is uncertain if the ground will return to its previous state. The practice of using historical albedo measurements of an empty site to make predictions of bifacial yield is therefore inherently uncertain and ongoing monitoring of site albedo after installation is required. Remote sensing cannot be used to measure albedo of a site after installation of a PV system unless an area is set aside for this purpose, as the PV modules obscure the view. Further studies are necessary to investigate such challenges.

Declaration of Competing Interest

The authors declare that they have no known competing financial interests or personal relationships that could have appeared to influence the work reported in this paper.

Acknowledgements

This work has received funding from the UK Department for Business Energy and Industrial Strategy through Innovate UK's "Analysis for Innovators Round 7" programme and through the UK National Measurement System.

The authors thank Niall Origo of the National Physical Laboratory for reviewing this work.

Author contribution statement.

JCB wrote the manuscript, wrote and implemented algorithms for calculation of albedo and performed analysis of data. GK and JCB designed the outdoor measurement system and experiment. GK, JCB, DP, NAM, SB and MR contributed to the design and planning of experiments, review of experimental results and data analysis. NAM and MR performed additional implementation of albedo algorithms and validation of algorithm outputs. DP and MR performed additional analysis of Sentinel-2 image data. All authors contributed to the review of this manuscript.

References

[1] R. Kopecek, J. Libal, Towards large-scale deployment of bifacial photovoltaics, Nat. Energy 3 (6) (2018) 443–446.
[2] VDMA, "International Technology Roadmap for Photovoltaic (ITRPV)," Frankfurt am Main, Germany, 2022. Available from https://www.vdma.org/international-technology-roadmap-photovoltaic.
[3] T.C.R. Russell, et al., The Influence of Spectral Albedo on Bifacial Solar Cells: A Theoretical and Experimental Study, IEEE J. Photovoltaics 7 (6) (2017) 1611–1618.
[4] N. Riedel-Lyngskær, et al., The effect of spectral albedo in bifacial photovoltaic performance, Sol. Energy 231 (2022) 921–935.
[5] Blakesley, J.C., et al., *Effective spectral albedo from satellite data for bifacial gain calculations of PV systems,* Proc. EUPVSEC 2020 (2020), DOI 10.4229/EUPVSEC20202020-5CO.9.3.
[6] M.R. Vogt, et al., Impact of Using Spectrally Resolved Ground Albedo Data for Performance Simulations of Bifacial Modules. (2018) 1011–1016.
[7] A.M.G. Amillo, et al., Application of Satellite-Based Spectrally-Resolved Solar Radiation Data to PV Performance Studies, Energies 8 (5) (2015) 3455–3488.
[8] C.A. Gueymard, et al., Surface albedo and reflectance: Review of definitions, angular and spectral effects, and intercomparison of major data sources in support of advanced solar irradiance modeling over the Americas, Sol. Energy 182 (2019) 194–212.
[9] R.R. Cordero, et al., Evaluation of MODIS-derived estimates of the albedo over the Atacama Desert using ground-based spectral measurements, Sci. Rep. 11 (1) (2021).
[10] Bailey, R., et al., *Investigations of site-specific, long term average albedo determination for accurate bifacial system energy modeling*, in *2019 IEEE 46th Photovoltaic Specialists Conference (PVSC)*. 2019, IEEE.
[11] J.A. Augustine, J.J. Deluisi, C.N. Long, SURFRAD-A National Surface Radiation Budget Network for Atmospheric Research ", *Am.* Meteorol. Soc (2000) 81.
[12] B. Marion, Measured and satellite-derived albedo data for estimating bifacial photovoltaic system performance, Sol. Energy 215 (2021) 321–327.
[13] https://modis.ornl.gov/.
[14] Schaaf, C. and Z. Wang, *MCD43A1 MODIS/Terra+Aqua BRDF/Albedo Model Parameters Daily L3 Global - 500m V006*. 2015, NASA EOSDIS Land Processes DAAC.
[15] M. Bouvet, et al., RadCalNet: A Radiometric Calibration Network for Earth Observing Imagers Operating in the Visible to Shortwave Infrared Spectral Range. 11 (20) (2019) 2401.
[16] M. Mira, et al., The MODIS (collection V006) BRDF/albedo product MCD43D: Temporal course evaluated over agricultural landscape, Remote Sens. Environ. 170 (2015) 216–228.
[17] C. Wu, et al., Ecohydrological effects of photovoltaic solar farms on soil microclimates and moisture regimes in arid Northwest China: A modeling study, Sci. Total Environ. 802 (2022), 149946.
[18] D. Uldrijan, et al., Ecological effects of preferential vegetation composition developed on sites with photovoltaic power plants, Ecol. Eng. 168 (2021), 106274.
[19] *Open access hub*. Available from: .
[20] IEC 61724-1:2021 *Photovoltaic System Performance Part 1: Monitoring.*, IEC (2021).
[21] *SILICON IRRADIANCE SENSOR*. Available from: https://www.imt-solar.com/fileadmin/docs/en/products/Si-Sensor_202205_E.pdf.
[22] *USER MANUAL SR20-D2*. Available from: https://www.hukseflux.com/uploads/product-documents/SR20-D2_manual_v2012.pdf.
[23] N. Martin, J.M. Ruiz, Calculation of the PV modules angular losses under field conditions by means of an analytical model (vol 70, pg 25, 2001), Sol. Energy Mater. Sol. Cells 110 (2013), 154-154.
[24] W. Lucht, C.B. Schaaf, A.H. Strahler, An algorithm for the retrieval of albedo from space using semiempirical BRDF models, IEEE Trans. Geosci. Remote Sens. 38 (2) (2000) 977–998.
[25] I. Reda, A. Andreas, Solar position algorithm for solar radiation applications, Sol. Energy 76 (5) (2004) 577–589.
[26] IEC 60904-3:*2019. Photovoltaic devices – Part 3: Measurement principles for terrestrial photovoltaic (PV) solar devices with reference spectral irradiance data. Edition 4.0 International Electrotechnical Commission*. IEC (2019).
[27] National Solar Radiation Database available from https://nsrdb.nrel.gov/.
[28] European Centre for Medium Range Weather Forecasting available from https://www.ecmwf.int/en/forecasts/datasets.
[29] Bird, R.E. and R.L. Hulstrom, *Simplified clear sky model for direct and diffuse insolation on horizontal surfaces*. (1981). doi:10.2172/6510849.
[30] D.T. Reindl, W.A. Beckman, J.A. Duffie, Diffuse fraction correlations, Sol. Energy 45 (1) (1990) 1–7.
[31] Using the pvl_reindl_2 PVLib MATLAB implementation from the PV Performance Modelling Colelctive (PVPMC) courtesy Sandia National Laboratory https://pvpmc.sandia.gov/.
[32] *About Copernicus*. Available from: https://www.copernicus.eu/en/about-copernicus.
[33] Konings, J. and A. Habte, *Uncertainty evaluation of measurements with pyranometers and pyrheliometers*, in *Proceedings of the ISES Solar World Congress 2015*. 2016, International Solar Energy Society.
[34] BIPM, *Guide to expression of uncertainty in measurement (GUM)*. JCGM 100:2008, 2008.
[35] Gostein, M., B. Marion, and B. Stueve, *Spectral Effects in Albedo and Rearside Irradiance Measurement for Bifacial Performance Estimation*. 2020.
[36] M.O. Roman, et al., Use of In Situ and Airborne Multiangle Data to Assess MODIS- and Landsat-Based Estimates of Directional Reflectance and Albedo, IEEE Trans. Geosci. Remote Sens. 51 (3) (2013) 1393–1404.
[37] J. Liu, et al., Validation of Moderate Resolution Imaging Spectroradiometer (MODIS) albedo retrieval algorithm : Dependence of albedo on solar zenith angle, J. Geophys. Res. 114 (2009).
[38] X. Wu, et al., Accuracy Assessment on MODIS (V006), GLASS and MuSyQ Land-Surface Albedo Products: A Case Study in the Heihe River Basin, China, Remote Sens. (Basel) 10 (12) (2018) 2045.
[39] MODIS MCD43A2 File Specification V6.1.0, available from https://ladsweb.modaps.eosdis.nasa.gov/filespec/MODIS/61/MCD43A2.
[40] M.J. Reno, C.W. Hansen, Identification of periods of clear sky irradiance in time series of GHI measurements, Renew. Energy 90 (2016) 520–531.
[41] Using the pvl_detect_clear_time MATLAB implementation from the PV Performance Modelling Colelctive (PVPMC) courtesy Sandia National Laboratory https://pvpmc.sandia.gov/.